Editors' Suggestion   Featured in Physics

Buckling-Fracture Transition and the Geometrical Charge of a Crack

Yael Klein and Eran Sharon

The Racah Institute of Physics, The Hebrew Univewrsity of Jerusalem, Jerusalem, 91904, Israel

We present a unifying approach that describes both surface bending and fracture in the same geometrical framework. An immediate outcome of this view is a prediction for a new mechanical transition: the buckling-fracture transition. Using responsive gel strips that are subjected to nonuniform osmotic stress, we show the existence of the transition: Thin plates do not fracture. Instead, they release energy via buckling, even at strains that can be orders of magnitude larger than the Griffith fracture criterion. The analysis of the system reveals the dependence of the transition on system's parameters and agrees well with experimental results. Finally, we suggest a new description of a mode I crack as a line distribution of Gaussian curvature. It is thus exchangeable with extrinsic generation of curvature via buckling. The work opens the way for the study of mechanical problems within a single nonlinear framework. It suggests that fracture driven by internal stresses can be completely avoided by a proper geometrical design.

Thin elastic sheets respond to stresses in various ways: long wavelength buckling, wrinkling [1–4], folding [5,6], and crumpling [7–10]. The most singular response to stress is fracture, which involves the separation of the material into fragments. While the phenomenology of buckling, wrinkling, and crumpling is studied within the framework of plate theories, cracking of thin plates is studied in a different framework—usually the linear elastic fracture mechanics (LEFM) [11,12].

An everyday example of cracking occurs when placing a hot glass cup on a cold marble table. The sharp temperature gradients within the cup lead to the buildup of stresses that can drive crack propagation. In a controlled experimental study of this phenomenon [13], a rectangular hot glass plate was dipped into a cold liquid in a fixed velocity. Depending on the dipping velocity, a single straight crack, a wavy crack, or several cracks propagated in the plate. Qualitatively similar phenomena were observed in other brittle materials [14]. Theoretical studies were mainly focused on understanding the wavy crack [15,16] or multiple crack propagation [17].

In what follows, we show that the dipped plate experiment is very similar to a different set of mechanical problems that was recently studied: the problem of non-Euclidean plates (NEPs). NEPs are thin elastic plates with intrinsic, non-Euclidean two-dimensional (2D) geometry. Such plates can be generated via nonuniform swelling [18–21], via growth of living tissue [22–24], or through plastic deformation [25,26]. NEPs were studied within the framework of incompatible elasticity. The in-plane inelastic deformation prescribes a reference metric field $\bar{g}(x, y)$ on the midplane of the plate, a metric field that encodes the local in-plane equilibrium distances between material elements. The reference metric can be non-Euclidean

namely, it determines via Gauss *Theorema Egregium*, a non-zero reference Gaussian curvature $\bar{K}$. In such cases, the plate's *s* equilibrium configuration is set by the competition between the bending and stretching energies [27]. The bending energy density is proportional to the cubic power of the thickness h and a quadratic function of the local curvatures. The stretching energy density is linear in h and a quadratic function of the in-plane strain, which is expressed as the difference between the reference metric and the actual metric of a configuration: $E_S \propto (g - \bar{g})^2$ [27]. This implies that stretch-free configurations are those in which $g = \bar{g}$. Since the Gaussian curvature is the only local invariant quantity of a 2D metric [28], a stretch-free configuration requires $K = \bar{K}$ everywhere. Likewise, a local deviation of K from $\bar{K}$ is a source of in-plane elastic strain. Experiments in responsive gel sheets [18–20] confirmed this assertion: In the thin limit, NEP indeed buckled and settled very close to embeddings of the reference metric with $K = \bar{K}$ nearly everywhere.

The glass plate in the dipping experiment is in fact a non-Euclidean plate. The local temperature profile defines via thermal expansion local equilibrium distances, i.e., a reference metric. The reference metric in these experiments is invariant parallel to the water-air interface (the x direction) depending only on the distance y from it

$$\bar{g}(y) = \begin{pmatrix} f^2(y) & 0 \\ 0 & 1 \end{pmatrix}, \qquad (1)$$

where $f(y)$ is the relative horizontal expansion at distance y from the water-air interface (measured on the deformed sheet). The reference Gaussian curvature prescribed by such metrics is given by (see Ref. [28])

$$\bar{K}(y) = -\frac{f''}{f}. \tag{2}$$

NEPs with such metrics were studied extensively [25,26,29–31] and were found to buckle and wrinkle. An immediate question would be the following: Why do the glass plates break, while gel sheets with a similar type of reference metric buckle? In addition, can the reduction of in-plane strain due to crack propagation be described as an approach of an actual metric to a reference one? If so, can we define a geometrical "charge" of Gaussian curvature to a crack and can it be related to conventional parameters of LEFM?

To address these questions, we designed an experimental setup which allows the investigation of the problem over a wide range of the relevant parameters. It consists of flat strips of polyacrylamide gel, which are immersed vertically in a thick water layer floating on top of a concentrated solution of polyethylene glycol (PEG4000) in water (25%–30% by weight). The sheets are slowly dipped into the PEG (typical speed $v \approx 3$ mm/h) [Fig. 1(a))]. The large PEG molecules cannot penetrate the fine porous gel; thus, water flows out of the gel to balance the osmotic pressure. As a result, the gel assumes a new reference volume within the PEG solution, which is significantly smaller than the equilibrium volume within water. In this way, the nonuniform PEG concentration profile defines a non-Euclidean reference metric of the form of Eq. (1), with $f(y)$ being the swelling factor at distance y from the water-PEG interface. It is of the form of a smoothed step function characterized by the normalized ratio of strip widths in the water and PEG regions: $\Delta \equiv [(f_{\text{water}} - f_{\text{PEG}})/f_{\text{PEG}}]$, and the length of the transition layer between them, l [Fig. 1(b))]. For such a metric, the reference curvature is zero away from the interface and it is of magnitude $\bar{K} \sim (\Delta^2/l^2)$ in the transition region (positive or negative in the water or PEG regions).

At long times, PEG molecules diffused into the water and the transition region $l(t)$ widened. Therefore, in each experiment, the gel strip went through a sequence of reference metrics $\bar{g}(t)$. In the reported experiments, we used strips of constant length (15 cm) and varied the width and thickness in the ranges 2–5 cm and 0.1–2 mm, respectively. The value of Δ was 0.32 ± 0.01 and l was varied from ∼1 mm (in the beginning of an experiment) to ∼10 mm (at the final stages of the experiments). One or more vertical notches were inserted in the bottom horizontal edge of the strips to allow crack propagation. As the gel strips were dipped into the PEG, we measured their configurations (every 10 min) using laser tomography [Fig. 1(c)) and Methods section in the Supplemental information file [32]].

The non-Euclidean gel strips showed a transition between two qualitatively different behaviors. Some of them behaved like the glass plates in Ref. [13]; they
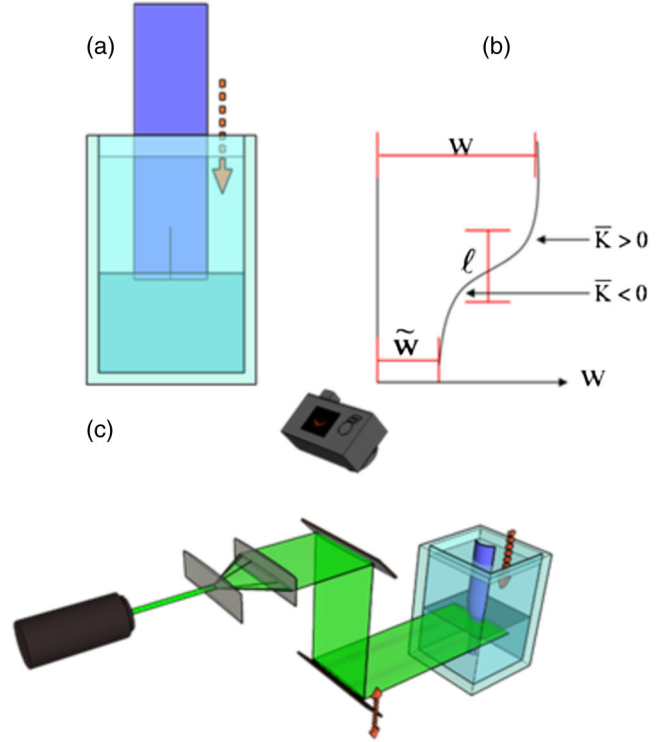

FIG. 1. Schematics of the experimental system. (a) A polyacrylamide gel strip is immersed into a stratified fluid. The top layer of the fluid is 100% water. The bottom layer is 25% PEG4000 in water. In the transition region, the osmotic pressure gradient prescribes a non-Euclidean metric on the sheet. (b) An illustration of the reference strip widths that are induced by the PEG concentration profile. The parameter Δ used in the text is defined as $\Delta \equiv [(W - \tilde{W})/\tilde{W}]$. Regions of positive and negative reference Gaussian curvature are marked on the figure. (c) Scanning laser sheet illuminates the gel. A camera captures the signal from fluorescent powder within the sheet, allowing the construction of its 3D configuration (see Methods section in the Supplemental information file [32] for details).

remained flat and cracks propagated in them. We observed strips with a single straight crack, with a single wavy crack, or with several propagating cracks [Fig. 2(a)]. The second type of behavior was buckling. The immersed strips buckled into 3D bottlelike configurations approaching the non-Euclidean reference metric by bending. In some of the plates, we found a combination of the two behaviors: The strips slightly buckled and a crack propagated in them. The mode of deformation of the sheets was correlated with their thickness. Very thin plates buckled, and no cracks propagated in them [Fig. 2(a) left]. At larger thicknesses, we found less bending of the strips, with still no crack propagation [Fig. 2(a) second from the left]. At further larger thickness, we observed crack propagation together with a significant decrease in the bending content [Fig. 2(a) middle]. At the largest thickness and widths, we observed more complex crack structures with no measurable surface bending [Fig. 2(a) right].
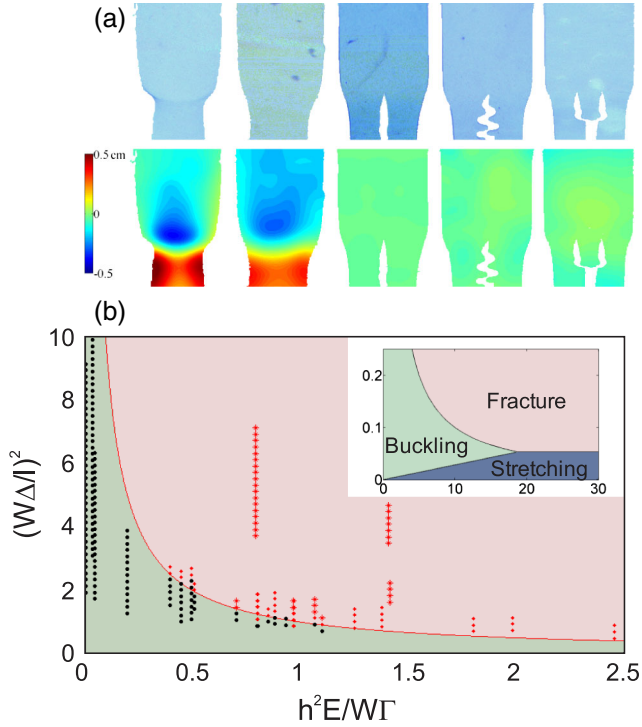
FIG. 2. Observation of a buckling-fracture transition. (a) Photos (top) and surface height measurements (bottom) of gel strips that are immersed into the PEG solution. Thin strips (left) buckle and do not support crack propagation. Thicker strips (right) hardly buckle. Instead, they are fractured by a straight or a wavy crack, or by several propagating cracks (extreme right). Strip thickness (left to right): 100, 750, 1500, 1750, and 2100 μm. (b) Measurements of buckling-fracture transitions. Each vertical column of symbols indicates the number of propagating cracks along a single experiment. Black circles, no propagating cracks; red circles, a single propagating crack; red stars, two propagating cracks. The solid line is the theoretical transition line $\varepsilon_{FB} \sim [(W\Gamma)/(Eh^2)]$. Inset: schematics of the predicted phase diagram showing the buckling-dominated, the stretching-dominated, and the fracture-dominated regions. The curves separating these regions are $\varepsilon_{BS} \sim (h^2/W^2)$, $\varepsilon_{FS} \sim \sqrt{\Gamma/EW}$, and $\varepsilon_{FB} \sim [(W\Gamma)/(Eh^2)]$. The axes are as in the main figure.

The experimental results can be explained by the following scaling analysis. The total energy of a plate is $F = F_B + F_S + F_F$, where F_B is the bending energy, F_S is the stretching energy, and F_F is the fracture surface energy. Adopting the Griffith approach to crack propagation, we consider the effect of an infinitesimal dipping δy of the sheet into the PEG solution. Such dipping would cause an increase in the stretching energy since the sheet in its flat configuration does not obey its reference non-Euclidean metric. The strain estimated as the "inverse Laplacian" of the reference Gaussian curvature is $\varepsilon \propto W^2 \bar{K}$. The variation in the stretching energy is, therefore,

$$\delta F_S \propto EhW\delta y \left(\frac{(W\Delta)^2}{l^2} \right)^2. \tag{3}$$

A propagation of the crack by δy would lead to an increase of F_F by

$$\delta F_F \propto \Gamma h \delta y. \tag{4}$$

Finally, a complete relaxation of in-plane stresses by buckling (with the typical curvatures being $|\kappa_{1,2}| \approx \sqrt{|K|} \approx (\Delta/l)$) would cause an increase of F_B by

$$\delta F_B \propto W\delta y Eh^3 \frac{\Delta^2}{l^2}. \tag{5}$$

Here, E is the Young's modulus of the material and Γ is its fracture energy.

Depending on material parameters and the strain $\varepsilon \sim [(W\Delta)^2/l^2]$, one can identify limits in which the system is dominated by either of the modes: relaxation of in-plane strain by buckling, relaxation via fracturing, or remaining flat and complete, keeping the in-plane strain. Balancing δF_S with δF_B identifies the buckling-stretching transition $\varepsilon_{BS} \sim (h^2/W^2)$, which is the scaling of the threshold for buckling of a plate. Balancing δF_S with δF_F identifies the fracture-stretching transition $\varepsilon_{FS} \sim \sqrt{\Gamma/EW}$, which is the Griffith criterion (see Supplemental Material [32] Sec. 2). Finally, balancing δF_F with δF_B identifies a buckling-fracturing transition: $\varepsilon_{FB} \sim [(W\Gamma)/Eh^2]$. We obtain a 2D phase space, which includes all three behaviors [inset of Fig. 2(b)].

While the two first transitions are well known, the buckling-fracture transition and its scaling have not been reported or studied. Our experimental results [Fig. 2(b)] confirm the existence of this transition and its predicted scaling: No propagating cracks were observed below a transition strain (note that the scaling argument accounts only for the functional dependent of the transition, not to the exact value of the strain; the quantitative agreement presented in the figure is coincidental). Cracks would not propagate in thin enough plates that relaxed strain via buckling even for internal strains that can be an order of magnitude larger than the Griffith criterion [the horizontal line in the inset of Fig. 2b)]. Slightly above the transition curve, single straight cracks were found to propagate. Farther away into the fracture-dominant region, we found oscillating cracks and several simultaneously propagating cracks.

Examining individual experiments, we find a connection between cracking and surface bending: As long as the crack propagated, the strip was relatively flat, but once the crack arrested, the strip buckled and obtained a 3D configuration (see Video M1 in the Supplemental Material [32]). In order to study the fracture-buckling interplay, we estimate the energy that is channeled into fracturing and into buckling at each moment during specific experiments. The energy released by fracturing is proportional to the square of the stress intensity factor—the prefactor of the parabolic
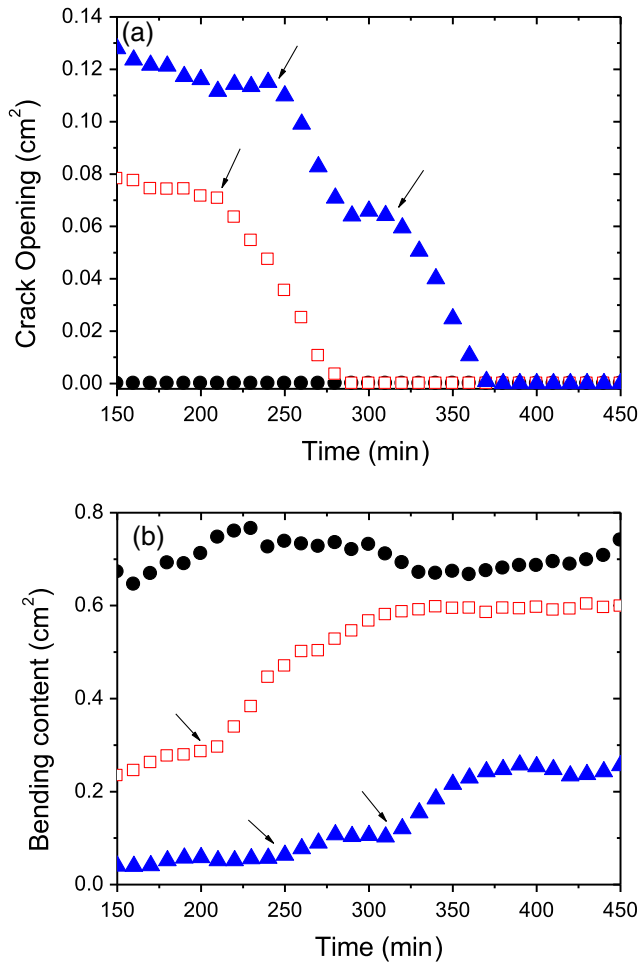
FIG. 3. Switching between fracturing and buckling. The crack opening (a) and average bending content (b) versus time plotted for propagating cracks in strips of thickness 1 mm (triangles), 0.85 mm (open squares), and 0.75 mm (circles). The 1 mm thick strip contained two propagating cracks and low bending content. Each crack arrest (indicated by arrows) was accompanied by an increase in the surface bending. The same process was observed in the 0.85 mm thick strip, which initially contained one propagating crack. No cracks propagated in the thinnest strip, which underwent the largest surface bending.

crack opening [11]—and can, therefore, be evaluated by measuring the crack opening, as defined in the Supplemental Material Sec. 2.4 [32]. The bending energy is proportional to the bending content—the integral of the square of surface curvature (see Supplemental Material Sec. 2.4 [32]). Both quantities are evaluated from an analysis of the 3D surface scans. We plot the crack opening [Fig. 3(a)] and the bending content [Fig. 3(b)] that were measured during three experiments using strips with different thicknesses. The 1 mm thick strip (blue triangles) initially contained two propagating cracks that stopped their propagation one after the other. Each of these crack-arrest events (indicated by arrows) was accompanied by an increase in the surface bending content and a (trivial) drop
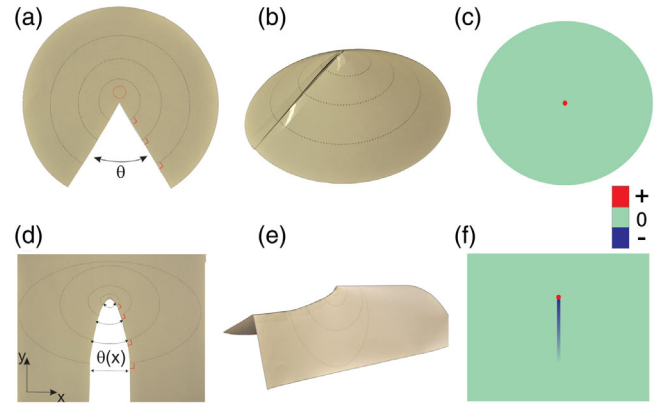

FIG. 4. Curved kirigami and the geometric charge of a crack. Flat configurations with cuts (left), bent configurations with edges identified (middle), and maps of the Gaussian curvature (right). A triangular cut (a) leads to a disk with a missing angle θ for any loop that surrounds the tip (dotted lines) but not for loops that do not surround the tip (red circle). (b) The geometry of a cone. (c) The Gaussian curvature of such geometry is zero, except for a singularity of $+\theta$ at the origin. In a typical "crack opening" profile (d), the missing angle at the tip is $+\pi$ and it decreases to zero (for a finite opening crack) away from the tip. The bent configuration (e) as well as the Gaussian curvature map (f) show a positive point singularity followed by a line singularity (a cusp) of negative curvature integrated to a total of $-\pi$. Such a representation of a crack includes all the information for the nonlinear elastic problem.

in the total crack opening. The 0.85 mm strip (open squares) started with a moderate bending content and one propagating crack. As in the former measurement, crack arrest was accompanied by a significant increase in the bending content. The thinnest strip (0.75 mm red symbols) had no propagating cracks from the very beginning. Its bending content was high throughout the entire experiment. These measured dynamic transitions imply that buckling and fracturing serve a similar geometrical task and can, to some level, be exchanged.

The results above motivate a geometric formulation of the crack propagation problem: It is well accepted that non-Euclidean plates reduce in-plane strain via buckling, which generates surface Gaussian curvature $K(\mathbf{r})$ close to $\bar{K}(\mathbf{r})$, the reference Gaussian curvature. In fact, within the formalism of incompatible elastic sheets, it is the only way internal stresses can be relaxed. The observed exchangeability between cracking and buckling hints that crack opening can be described as a distribution of Gaussian curvature. As known from studies of kirigami [33], point singularities of Gaussian curvature can be generated by closing straight cuts. Such a process changes the reference geometry of the sheet, i.e., it changes $\bar{K}(\mathbf{r})$. Fracture differs in two main aspects: It is a generation of actual (rather than reference) Gaussian curvature $K(\mathbf{r})$ distribution, and it is not limited to point singularities. The curved crack opening profile is equivalent to a "curved

kirigami." It can be shown using the Gauss-Bonnet theorem (see Supplemental Material Sec. 2.6 [32]) that this leads to line singularity of negative Gaussian curvature along the crack edges. Using a kirigamilike method, we demonstrate the geometry encoded in a surface with curved cuts (Fig. 4). Increasing the number of cuts allows us to approach a non-Euclidean smooth geometry with a pricewise Euclidean sheet (Supplemental Material Fig. S3 [32]).

Viewing a mode I crack as a line distribution of Gaussian curvature allows us to treat cracking and buckling phenomena in a similar framework. Unlike the case of intrinsic singularities, such as dislocations whose geometry is encoded in $\bar{g}$, bringing it closer to a defined imposed configuration [34], the crack geometry is part of the *response* of the body. Therefore, it is a property of the actual metric g. For example, the elastic energy in an intrinsically flat sheet (Euclidean $\bar{g}$) draped on a curved surface (non-Euclidean g) can be reduced by inserting cracks [35], which makes g closer to Euclidean. In our experiments, the sheets are free of external constraints. Therefore, they can "choose" to release stresses via buckling *or* fracture—two alternative ways of distributing Gaussian curvature. In the case of fracture, crack opening (and thus, the nonlinear strains) is selected as an optimal distribution of Gaussian curvature line singularity, which best approximates the reference Gaussian curvature. The selection of the preferred mode of deformation (buckling or fracture) is set by the parameters of the problem, somewhat similar to the selection between elastic and inelastic deformations of constrained sheets that was studied in Ref. [36]. In the present case, however, the nucleation or propagation cost of the geometry-carrying entity is that of a fracture, and it competes with the cost of global surface bending, leading to the specific scaling of the transition. A direct outcome of this view is that fracturing due to residual stresses can be *completely avoided* by proper tuning of geometrical dimensions of the body—mainly its thickness [an increase of 1 order of magnitude in the critical strain for fracture is demonstrated in Fig. 2b)]. This observation might open the way for new technologies that will reduce aging (due to internal stresses) of energy storing devices. On a more basic level, having fracture and buckling described within a single nonlinear formalism provides the way to handle problems that involve these two modes of deformation and to directly obtain the (nonuniversal) higher order and nonlinear terms of the stress around crack tips. Finally, combining the geometrical view of fracture with new methods of solving the nonlinear plane-stress problem [37] seems to be an excellent framework for solving systems of interacting cracks, which are extremely difficult to handle within linearized theories.

[1] N. Bowden, S. Brittain, A. G. Evans, J. W. Hutchinson, and G. M. Whitesides, Spontaneous formation of ordered structures in thin films of metals supported on an elastomeric polymer, Nature (London) **393**, 146 (1998).

[2] E. Cerda and L. Mahadevan, Geometry and Physics of Wrinkling, Phys. Rev. Lett. **90**, 074302 (2003).

[3] J. Huang, M. Juszkiewicz, W. H. de Jeu, E. Cerda, T. Emrick, N. Menon, and T. P. Russell, Capillary wrinkling of floating thin polymer films, Science **317**, 650 (2007).

[4] B. Davidovitch, R. D. Schroll, D. Vella, M. Adda-Bedia, and E. A. Cerda, Prototypical model for tensional wrinkling in thin sheets, Proc. Natl. Acad. Sci. U.S.A. **108**, 18227 (2011).

[5] L. Pocivavsek, R. Dellsy, A. Kern, S. Johnson, B. Lin, K. Y. C. Lee, and E. Cerda, Stress and fold localization in thin elastic membranes, Science **320**, 912 (2008).

[6] H. Diamant and T. A. Witten, Compression Induced Folding of a Sheet: An Integrable System, Phys. Rev. Lett. **107**, 164302 (2011).

[7] T. A. Witten, Stress focusing in elastic sheets, Rev. Mod. Phys. **79**, 643 (2007).

[8] H. Aharoni and E. Sharon, Direct observation of the temporal and spatial dynamics during crumpling, Nat. Mater. **9**, 993 (2010).

[9] M. BenAmar and Y. Pomeau, Crumpled paper, Proc. R. Soc. A **453**, 729 (1997).

[10] G. A. Vliegenthart and G. Gompper, Forced crumpling of self-avoiding elastic sheets, Nat. Mater. **5**, 216 (2006).

[11] L. B. Freund, *Dynamic Fracture Mechanics* (Cambridge University Press, Cambridge, England, 1990).

[12] K. B. Broberg, *Cracks and Fracture* (Academic Press, London, 1999).

[13] A. Yuse and M. Sano, Transition between crack patterns in quenched glass plates, Nature (London) **362**, 329 (1993).

[14] R. D. Deegan, S. Chheda, L. Patel, M. Marder, H. L. Swinney, J. Kim, and A. de Lozanne, Wavy and rough cracks in silicon, Phys. Rev. E **67**, 066209 (2003).

[15] M. Marder, Instability of a crack in a heated strip, Phys. Rev. E **49**, R51 (1994).

[16] M. Addabedia and Y. Pomeau, Crack instabilities of a heated glass strip, Phys. Rev. E **52**, 4105 (1995).

[17] T. Boeck, H. A. Bahr, S. Lampenscherf, and U. Bahr, Self-driven propagation of crack arrays: A stationary two-dimensional model, Phys. Rev. E **59**, 1408 (1999).

[18] Y. Klein, E. Efrati, and E. Sharon, Shaping of elastic sheets by prescription of non-Euclidean metrics, Science **315**, 1116 (2007).

[19] Y. Klein, S. Venkataramani, and E. Sharon, Experimental Study of Shape Transitions and Energy Scaling in Thin Non-Euclidean Plates, Phys. Rev. Lett. **106**, 118303 (2011).

[20] J. Kim, J. A. Hanna, M. Byun, C. D. Santangelo, and R. C. Hayward, Designing responsive buckled surfaces by half-tone gel lithography, Science **335**, 1201 (2012).

[21] M. E. McConney, A. Martinez, V. P. Tondiglia, K. M. Lee, D. Langley, I. I. Smalyukh, and T. J. White, Topography from topology: Photoinduced surface features generated in liquid crystal polymer networks, Adv. Mater. **25**, 5880 (2013).

[22] U. Nath, B. C. W. Crawford, R. Carpenter, and E. Coen, Genetic control of surface curvature, Science **299**, 1404 (2003).

[23] E. Sharon, M. Marder, and H. L. Swinney, Leaves, flowers and garbage bags: Making waves, Am. Sci. **92**, 254 (2004).

[24] M. Arroyo and A. DeSimone, Shape control of active surfaces inspired by the movement of euglenids, J. Mech. Phys. Solids **62**, 99 (2014).

[25] E. Sharon, B. Roman, M. Marder, G. S. Shin, and H. L. Swinney, Mechanics: Buckling cascades in free sheets—Wavy leaves may not depend only on their genes to make their edges crinkle, Nature (London) **419**, 579 (2002).

[26] E. Sharon, B. Roman, and H. L. Swinney, Geometrically driven wrinkling observed in free plastic sheets and leaves, Phys. Rev. E **75**, 046211 (2007).

[27] E. Efrati, E. Sharon, and R. Kupferman, Elastic theory of unconstrained non-Euclidean plates, J. Mech. Phys. Solids **57**, 762 (2009).

[28] B. O'Neill, *Elementary Differential Geometry*, 2nd ed. (Academic Press, New York, 1997).

[29] J. A. Gemmer and S. C. Venkataramani, Shape selection in non-Euclidean plates, Physica (Amsterdam) **240D**, 1536 (2011).

[30] M. Marder and N. Papanicolaou, Geometry and elasticity of strips and flowers, J. Stat. Phys. **125**, 1065 (2006).

[31] B. Audoly and A. Boudaoud, Self-Similar Structures near Boundaries in Strained Systems, Phys. Rev. Lett. **91**, 086105 (2003).

[32] See Supplemental Material at http://link.aps.org/supplemental/10.1103/PhysRevLett.127.105501 for description of methods, calibrations, definitions and a supplemental video.

[33] T. Castle, Y. Cho, X. Gong, E. Jung, D. M. Sussman, S. Yang, and R. D. Kamien, Making the Cut: Lattice Kirigami Rules, Phys. Rev. Lett. **113**, 245502 (2014).

[34] W. T. M. Irvine, V. Vitelli, and P. M. Chaikin, Pleats in crystals on curved surfaces, Nature (London) **468**, 947 (2010).

[35] N. P. Mitchell, V. Koning, V. Vitelli, and W. T. M. Irvine, Fracture in sheets draped on curved surfaces, Nat. Mater. **16**, 89 (2017).

[36] G. M. Grason and B. Davidovitch, Universal collapse of stress and wrinkle-to-scar transition in spherically confined crystalline sheets, Proc. Natl. Acad. Sci. U.S.A. **110**, 12893 (2013).

[37] M. Moshe, E. Sharon, and R. Kupferman, Elastic interactions between two-dimensional geometric defects, Phys. Rev. E **92**, 062403 (2015).